OPTICAL CHARACTERIZATION OF THIN FILMS FOR SOLAR CELL APPLICATION

BY

AMENSISA ABDI

A THESIS

PRESENTED TO

THE SCHOOL OF GRADUATE STUDIES OF

ADDIS ABABA UNIVERISTRY

IN PARTIAL FULFILLMENT OF

THE REQUIREMENT FOR THE DEGREE

MASTER OF SCIENCE IN PHYSICS

JUNE 1995

ADDIS ABABA

ABSTRACT

Reflectance (R) and Transmittance (T) measurements can provide information about optical properties of thin films. Optical characteristic of different transparent conducting oxides (TCOs) have been studied. Optical band gap of hydrogenated amorphous silicon and hydrogenated amorphous silicon alloys thin films are calculated from R & T measurements using Hishikawa's relation and the program we have written. Thickness, optical band gap and dielectric function of a-Si:H films can be obtained at a time from R and T measurements using an optical simulation soft ware for layer stacks. Near normal incidence R data is fitted with a model to obtain dielectric function and from the obtained result T curve is simulated to prove whether the obtained dielectric function represents the film or not. This method can be extended even to non-transparent films. To characterize non-transparent films, however, is necessary to perform R_s (s - polarized) and R_p (p - polarized) measurements for incidence angle different from near normal incidence (6°) angle. p-i-n solar cell has been characterized by the same method with a model.

ACKNOWLEDGEMENTS

I would like to express my heart felt gratitude to Prof. H.Wagner who has enabled me to join the Solar Cell Characterization research group at the Institute of Thin Films and Ion Technology (ISI-PV), KFA-Juelich, Germany.

I am also greatly indebted to my advisor Dr. Th. Eickhoff for his consistent advise, guidance and friendly encouragement throughout the work.

Also my thanks go to Ms. K. Winz & Mr. B. Rech for their practical assistance and unreserved help in facilitating the work.

I extend my warmest gratitude to all members of the Solar Cell Characterization group in KFA-Juelich for their unreserved assistance.

I Would like to thank my brother Ashebir Fisera and my friends Aynalem H/Micheal, Takele Seda, Agebe Ligaba, and Mulugeta Libise, for their help and encouragement throughout my study.

I am thankful to Dr. F. Dworschack for his help in finding a qualified and appropriate advisor in the field I proposed.

It is my pleasure to thank my Advisor in Ethiopia Dr. Uli Stutenbaeumer for his valuable comments and suggestions.

Finally, I would like to thank DAAD for financing my postgraduate study.

CONTENT

1. INTRODUCTION

Photovoltaic, the conversion of sunlight directly into electricity using solar cells, is one of the most environmentally safe and renewable energy options for the world [1]. Hydrogenated amorphous silicon (a-Si:H) and its alloys thin film solar cells have got attention for covering large area with low cost [2]. The optical and electronic properties of a-Si:H are suitable for its application in the areas of photovoltaic and electronics devices such as: the low cost thin film solar cells, electrophotographic devices, image sensors and thin film transistors [3-6]. Moreover, deposition of a-Si:H and its alloys multi-layer thin film solar cells using modern semiconductor technology is easy. Thus, the research interest of a-Si:H for its importance in producing low cost solar cells has been continuously growing [2,4,5].

a-Si:H and its alloys thin film solar cells show a promising new approach for low cost solar cell development. A world record solar cell performance of 10.2% with stable conversion efficiency has been achieved by United Solar System Corp. (USSC), American joint venture between Energy Conversion Device Inc. (ECD), and Canon Inc. on a multi-junction amorphous silicon alloy solar panel [1].

Therefore, to improve the conversion efficiency of a-Si:H solar cells, precise cell design based on the knowledge of optical constants of the material is essential [4,5,7]. Nowadays, in order to optimize the design of solar cells, it becomes a prerequisite to understand the optical characteristics of individual layers in particular and the cell as the whole [3-6,8,9]. The method often chosen to determine the optical constants of materials is by measuring the intensity of reflected (R) and transmitted (T) light [9-14]. That is measuring R and T, and determining optical band gap (E_g), dielectric function $\tilde{\epsilon} = \epsilon_1 - i\epsilon_2$, and thickness of the film (d) therefrom.

In our work, Perkin Elmer Lambda 19 UV/VIS/NIR double beam spectrophotometer was used to perform R and T measurements of thin films. And then, the program we have written in TransEra HTBasic software was used for interference free determination of α after

Hishikawa's relation (α=(-1/d)*ln(T/(1-R))) and to prepare data for Tauc's plot. The optical band gap (E_g) was determined from Tauc's plot (i.e. from plot of sqrt($\alpha h\nu$) Vs $h\nu$). R data were fitted using an optical simulation software for layer stacks called window version software for variable angle spectroscopic ellipsometer (W.V.A.S.E) data. From the fitting result, thickness (d), E_g, optical functions refractive index (n) and absorption index (κ) or dielectric functions $\tilde{\epsilon} = \epsilon_1 - i\epsilon_2$ were obtained. To prove, if one has received a definite set of parameters for $\tilde{\epsilon}$ together with the thickness d from R-fitting, one has to check if the obtained parameter set describes the T-measurement.

In section 2, fundamental theory of R and T, and Fresnel's relations are discussed. General Fresnel's relations, and their relations to R and T in particular case for polarized light incident on the plane interface is included. R and T of thin film are also presented. Section 3 contains a list of experimental apparatus and procedures to carry out measurements. In the fourth section the results of the work are presented and the interpretation of the graphs are given. Optical design of multi-layered a-Si:H thin film solar cells requires not only understanding of the complete cell, but also understanding of absorption in its individual layers [4,5]. In section 4, individual layers used in p-i-n a-Si:H solar cell and the complete cell itself are characterized. And finally, in sections 5 and 6 conclusions and reference materials are stated.

2. THIN FILM OPTICS

Absorption is an important thin film phenomenon that can give information about electronic structure of solids [3,4,7]. The accurate, fast and powerful method for the determination of optical absorption coefficient (α), optical energy gap (E_g) and optical constants of thin film is from the measurement of reflectance (R) and transmittance (T) [7,12-14]. So, the discussion about transmittance, reflectance and absorbance in this chapter is worthwhile. In the following sections we will consider R, T and α of thin films based on the electromagnetic theory of light. The electromagnetic waves considered are basically the solutions of the boundary value problems of electromagnetic wave equations.

2.1 Reflectance and transmittance at interface

In the foregoing discussion the following subscript:

- i for incident
- r for reflected
- t for transmitted
- 0 for amplitude
- $\parallel$ for parallel

and - $\perp$ for perpendicular

are used throughout the paper.

The electromagnetic fields, electric field ($\vec{E}$) and magnetic field ($\vec{B}$) are interdependent. One can be expressed in term of the other. The Fresnel's relations are defined as follows.

Fresnel's amplitude transmission coefficient ($\tilde{t}$) is defined as the ratio of the amplitude of transmitted electric field (E_{0t}) to the amplitude of the incident electric field (E_{0i}). Whereas, Fresnel's amplitude reflection coefficient ($\tilde{r}$) is defined as the ratio of the amplitude of the reflected electric field (E_{0r}) to (E_{0i}).

Suppose a plane polarized and monochromatic wave is incident on a plane interface separating two isotropic media of uniform refractive index $\tilde{n}_i$ and $\tilde{n}_t$, $\tilde{t}$ and $\tilde{r}$ can be found from the conditions of $\vec{E}$ and $\vec{B}$ fields at the interface. Suppose a plane monochromatic wave

$$\vec{E}_i = \vec{E}_{0i} \exp\left[+i\left(\vec{k}_i \cdot \vec{r} - \omega t\right)\right] \tag{2.1.1}$$

is incident on an isotropic and homogeneous plane interface (Fig. 2.1),

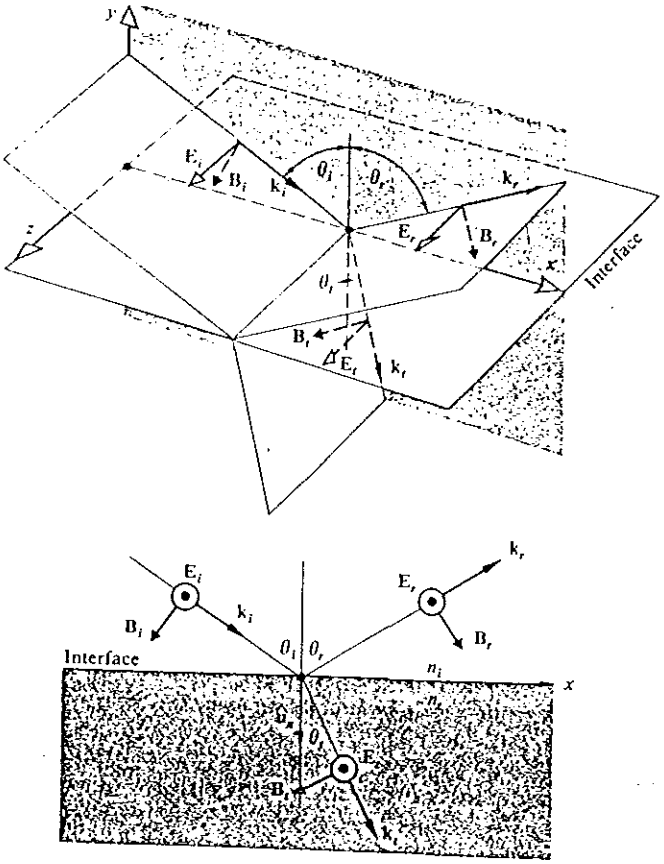

a) An incident E-field is normal to the plane of incidence.

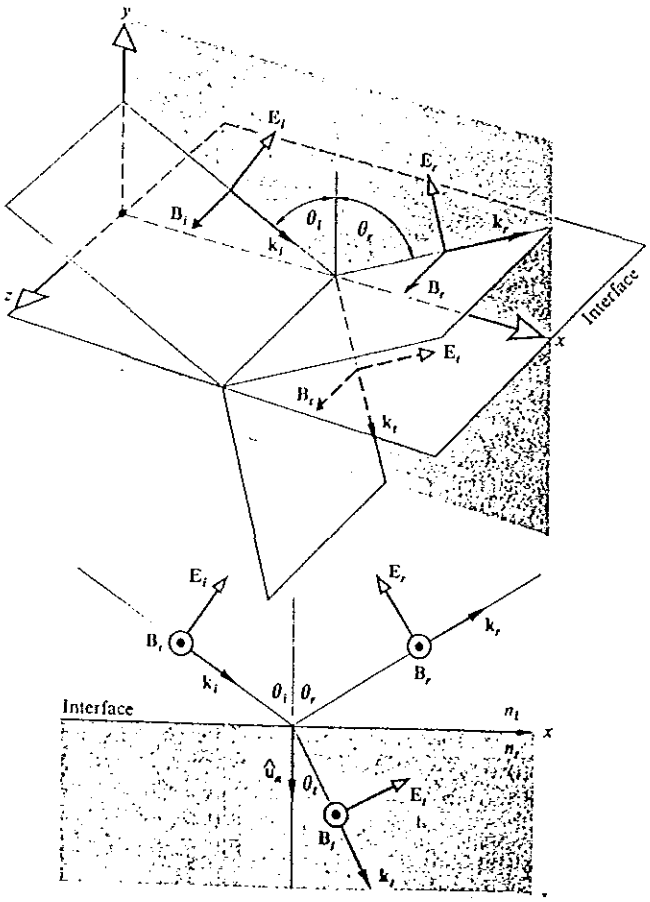

b) An incident E-field is parallel to the plane of incidence.

Fig. 2.1

then $\tilde{r}$ and $\tilde{t}$ are dependent on the orientation of the incident electric field ($\vec{E}_i$) with respect to the plane of incidence [15,16]. There are two cases: a) where electric field is parallel to the plane of incidence $(\vec{E}_i)_\parallel$ (p-polarized light) and b) where electric field is perpendicular to the plane of incidence $(\vec{E}_i)_\perp$ (s-polarized light). $\tilde{r}$ and $\tilde{t}$ in terms of generalized complex refractive index $\tilde{N}$ are as given by equations (2.1.3) and (2.1.4) below where the generalized complex refractive index ($\tilde{N}$) is given as

$$\tilde{N}_j = N_j + iK_j = \sqrt{\tilde{\epsilon}_j\mu_j - \sin^2\theta_i} \qquad (2.1.2)$$

where j can take two values: 0 (for the medium through which light is incident) or t (for transmitting medium) and θ_i is angle of incidence.

For normal incidence the generalized complex index of refraction reduces to complex refractive index of the material, i.e., $\tilde{N}_j = \tilde{n}_j = (\tilde{\epsilon}_j\mu_j)^{1/2}$

When the electric field ($\vec{E}$) is perpendicular to the plane of incidence (Fig. 2.1 a), $\tilde{r}_\perp$ and $\tilde{t}_\perp$ are as given by [17-19]:

$$\tilde{r}_\perp = \left(\frac{E_{0r}}{E_{0i}}\right)_\perp = \frac{\tilde{N}_i/\mu_i - \tilde{N}_t/\mu_t}{\tilde{N}_i/\mu_i + \tilde{N}_t/\mu_t} \qquad (a)$$

and (2.1.3)

$$\tilde{t}_\perp = \left(\frac{E_{0t}}{E_{0i}}\right)_\perp = \frac{2\tilde{N}_i/\mu_i}{\tilde{N}_i/\mu_i + \tilde{N}_t/\mu_t} \qquad (b)$$

while for the case when $\vec{E}$ is parallel to the plane of incidence, $\tilde{r}_{\parallel}$ and $\tilde{t}_{\parallel}$ are given as [10,13]:

$$\tilde{r}_{\parallel} = \left(\frac{E_{0r}}{E_{0i}}\right)_{\parallel} = \frac{\tilde{N}_i/\tilde{\epsilon}_i - \tilde{N}_t/\tilde{\epsilon}_t}{\tilde{N}_t/\tilde{\epsilon}_t + \tilde{N}_i/\tilde{\epsilon}_i} \qquad (a)$$

and (2.1.4)

$$\tilde{t}_{\parallel} = \left(\frac{E_{0t}}{E_{0i}}\right)_{\parallel} = \frac{2\tilde{N}_i/\tilde{\epsilon}_i}{\tilde{N}_t/\tilde{\epsilon}_t + \tilde{N}_i/\tilde{\epsilon}_i} \qquad (b)$$

Eqn. (2.1.3) and eqn. (2.1.4) are referred to as Fresnel's reflection and transmission amplitude coefficients for plane polarized electromagnetic wave.

For normal incidence where $\sin\theta_i = \sin\theta_t = 0$, there is no difference in the plane of polarization. Thus, for normal incidence, the Fresnel's relations satisfy:

$$\tilde{r}_{\parallel} = (-\tilde{r}_{\perp}) = \frac{\tilde{n}_t - \tilde{n}_i}{\tilde{n}_t + \tilde{n}_i} \qquad (a)$$

(2.1.5)

$$\tilde{t}_{\parallel} = \tilde{t}_{\perp} = \frac{2\tilde{n}_i}{\tilde{n}_t + \tilde{n}_i} \qquad (b)$$

and

$$\tilde{t}_{\parallel} + \tilde{r}_{\parallel} = 1 \qquad (c)$$

In eqn. (2.1.5) $\tilde{n}_i$ and $\tilde{n}_t$ are refractive indices of the materials.

Reflectance (R) and transmittance (T) are defined as a ratio of the reflected light intensity to the incident light intensity and a ratio of the transmitted light intensity to the incident light intensity respectively [15,16].

Intensity which is also known as flux density or irradiance is directly proportional to the square of the amplitude of electric field (disturbance). It is given by:

$$I_i = \frac{c\,\epsilon_0}{2} E_{0i}^2 \qquad (2.1.6)$$

where ϵ_0 is permittivity of free space and c is speed of light in vacuum.

For normal incidence, from definitions of R, T and eqn. (2.1.6) one can obtain the relation for R and T in terms of refractive indices of the materials as:

$$R = R_{\parallel} = R_{\perp} = \tilde{r}_{\parallel}\tilde{r}_{\parallel}^{*} = \left(\frac{\tilde{n}_t - \tilde{n}_i}{\tilde{n}_t + \tilde{n}_i}\right)\left(\frac{\tilde{n}_t - \tilde{n}_i}{\tilde{n}_t + \tilde{n}_i}\right)^{*} \qquad (a)$$

and

$$T_{\parallel} = \frac{\tilde{n}_t}{\tilde{n}_i}\tilde{t}_{\parallel}\tilde{t}_{\parallel}^{*} = \frac{\tilde{n}_t}{\tilde{n}_i}\left(\frac{2\tilde{n}_i}{\tilde{n}_i + \tilde{n}_t}\right)\left(\frac{2\tilde{n}_i}{\tilde{n}_t + \tilde{n}_i}\right)^{*} \qquad (b) \qquad (2.1.7)$$

The medium through which light is incident on the substrate is air. Therefore, $n_i = n_0$ is assumed to be real. For an absorbing substrate, $\tilde{n}_t$ should be replaced by its complex representation $\tilde{n}_t = n - i\kappa$. Substituting for $\tilde{n}_t$ and $\tilde{n}_i$, eqn (2.1.7) can be rewritten as:

$$R = \frac{(n - n_0)^2 + \kappa^2}{(n + n_0)^2 + \kappa^2} \qquad (a)$$

and

$$T = \frac{4n_0(n - i\kappa)}{(n + n_0)^2 + \kappa^2} \qquad (b) \qquad (2.1.8)$$

We have discussed Fresnel's relations, and relations of R and T at interface. In the next section let us extend our discussion to R and T of a single film.

2.2 Reflectance and transmittance by a single film

Consider Fig. 2.2,

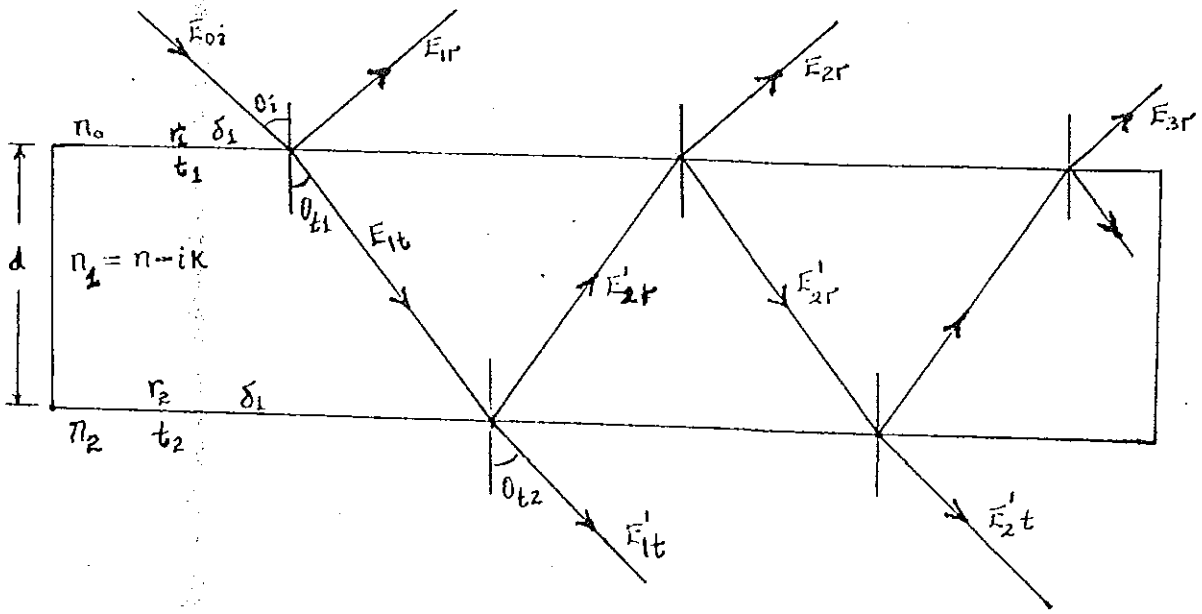

Fig. 2.2 Multiple reflection and transmission from a single film

a parallel and isotropic film of refractive index $\tilde{n}_1$ between media of refractive indices n_0 and n_2, the amplitude reflection ($\tilde{r}$) and transmission ($\tilde{t}$) can be obtained by summing multiply-reflected beams [16-19]. $\tilde{r}$ and $\tilde{t}$ are given by:

$$\tilde{r} = \frac{\tilde{r}_1 + \tilde{r}_2 \exp(-2i\delta_1)}{1 + \tilde{r}_1\tilde{r}_2 \exp(-2i\delta_1)} \qquad (a)$$

and (2.2.1)

$$\tilde{t} = \frac{\tilde{t}_1\tilde{t}_2 \exp(-i\delta_1)}{1 + \tilde{r}_1\tilde{r}_2 \exp(-2i\delta_1)} \qquad (b)$$

where $\tilde{t}_1$ and $\tilde{r}_1$ are Fresnel coefficients at the $n_0/\tilde{n}_1$ interface

$\tilde{t}_2$ and $\tilde{r}_2$ are Fresnel coefficient at $\tilde{n}_1/n_2$ interface

$\tilde{\delta}_1 = (2\pi/\lambda)d\tilde{K}_1$ is phase thickness $(\tilde{K}_1 = (\tilde{n}_1^2 - \sin^2\theta_1 t)^{1/2})$

d is thickness of the film and λ is vacuum wavelength.

Eqn. (2.2.1) holds for both cases when the electric field is parallel and perpendicular to the plane of incidence, i.e. for p-polarized and for s-polarized electric fields. One can obtain from eqn. (2.2.1), reflectance (R) and transmittance (T) of the single film as:

$$R = |\tilde{r}|^2 + \frac{|\tilde{t}|^4|\tilde{r}_2|^2\exp[-4Im(\delta_1)]}{1 - |\tilde{r}|^2|\tilde{r}_2|^2\exp[-4Im(\delta_1)]} \qquad (a)$$

and (2.2.2)

$$T = \left(\frac{n_2}{n_o}\right)\left(\frac{|\tilde{t}|^2|\tilde{t}_2|^2\exp[-2Im(\delta_1)]}{1 - |\tilde{r}|^2|\tilde{r}_2|^2\exp(-4Im(\delta_1)]}\right) \qquad (b)$$

Eqn. (2.2.2) is a general relation for R and T. It is valid for any type of film on a substrate.

2.3 Optical absorbance

Absorption is a phenomenon of fundamental interest because of its relation to the dynamics of electrons and ions of the medium which influence the electromagnetic radiation [3,4]. An absorbing medium is characterized by a complex dielectric function $\tilde{\epsilon} = \epsilon_1 - i\epsilon_2$ or very often by the complex refractive index $\tilde{n}_t = n - i\kappa$ which describes the propagation of an electromagnetic wave in the material is used instead [9,16]. Eqn. (2.1.1), an expression of $\vec{E}$ can be rewritten in terms of complex refractive index. For a wave moving in y-direction, using $K_y = \omega/u$ and $\tilde{n}_t = u/c$, it can be rewritten as:

$$\vec{E} = \vec{E_0}\exp(-\frac{\omega\kappa y}{c}) \times \exp(-i\omega(t + \frac{ny}{c})) \quad (2.3.1)$$

In absorbing media the light disturbance will proceed with a speed of c/n. As it progresses into the absorbing medium its amplitude is attenuated exponentially $[E_0\exp(-\omega\kappa y/c)]$. And the irradiance (I) which is proportional to the square of the amplitude of $\vec{E}$ is given by:

$$I = I_0 e^{-\alpha y} \quad (2.3.2)$$

where I_0 is the irradiance at an interface (y=0) and $\alpha = 2\omega\kappa/c$ is the absorption coefficient or the attenuation coefficient.

The inverse of α is known as penetration depth [15]. Penetration depth is the thickness for which the flux density (I) drops by a factor of 1/e. For a material to be transparent its penetration depth should be large compared to its thickness. Metals have exceedingly small penetration depth. Thus for materials to be transparent, their thickness must be very small.

For near normal incidence, T, R, d, and α are related according to Hishikawa [16] as given by eqn. (2.3.3)

$$\alpha = -\frac{1}{d}\ln\left(\frac{T}{1-R}\right) \quad (2.3.3)$$

The optical band gap (E_g) is usually determined from Tauc's plot. E_g is supposed to be the intercept of sqrt($\alpha h\nu$) Vs $h\nu$) plot. Two decades ago, Tauc derived the equation [20,21]

$$\omega^2\epsilon_2 \propto (h\nu - E_g)^2 \quad (2.3.4)$$

2.4 Dielectric functions

The response of dielectric materials to electromagnetic waves is of special concern to us in optics. An absorbing medium is characterized by a complex dielectric constant $\tilde{\epsilon} = \epsilon_1 - i\epsilon_2$, and complex refractive index $\tilde{n} = n - i\kappa$ [9,19].

The effect of introducing a homogeneous, isotropic dielectric material into the region of free space is to change ϵ_0 to $\tilde{\epsilon}$ and μ_0 to μ in Maxwell's equations. It follows from Maxwell's equations for free electrons that

$$(n - i\kappa)^2 = \epsilon_1 - i\epsilon_2 \qquad (2.4.1)$$

so that

$$\epsilon_1 = n^2 + \kappa^2 \quad \text{and} \quad \epsilon_2 = 2n\kappa$$

The spectral dependence of the refractive index and absorption index can be described by Cauchy, and Forouhi and Bloomer dispersion equation for amorphous material [20,21]. Simulating parameters with the dispersion equation to get a curve that fits the experimental data, one can precisely determine optical constants.

Tauc's relation eqn. (2.3.4) can be rewritten with the help of informations that $\epsilon_2 = 2n\kappa$ and $\alpha = 2\omega\kappa/c$ as:

$$\alpha h\nu \propto (h\nu - E_g)^2 \qquad (2.4.2)$$

To determine E_g of layers graphically, we used the concept of eqn. (2.4.2).

3. EXPERIMENTAL DETAILS

In this chapter, all experimental apparatus used are listed and the methods used are briefly discussed.

3.1 Experimental apparatus

R and T measurements were performed on Perkin Elmer Lambda 19 UV/VIS/NIR double beam spectrophotometer (Fig. 3.1). It measures the ratio of the intensities of two beams (i.e. ratio of the intensity of sample beam to intensity of reference beam). It is a fast and powerful machine for measuring reflectance (R) and transmittance (T) of layers. Parts of Lambda 19 and the instruments used with it are:

1. Main compartment of spectrophotometer
2. Normal reflectance accessory with:
   - two near normal incidence reflectance sample holders
   - two transmittance sample holders
   - two variable angle reflectance sample holders
   - standard mirrors with calibration data
3. 6 inch diameter integrating sphere with:
   - center mount sample holder
   - standard reflectance materials
4. PC computer with plotter
5. Samples

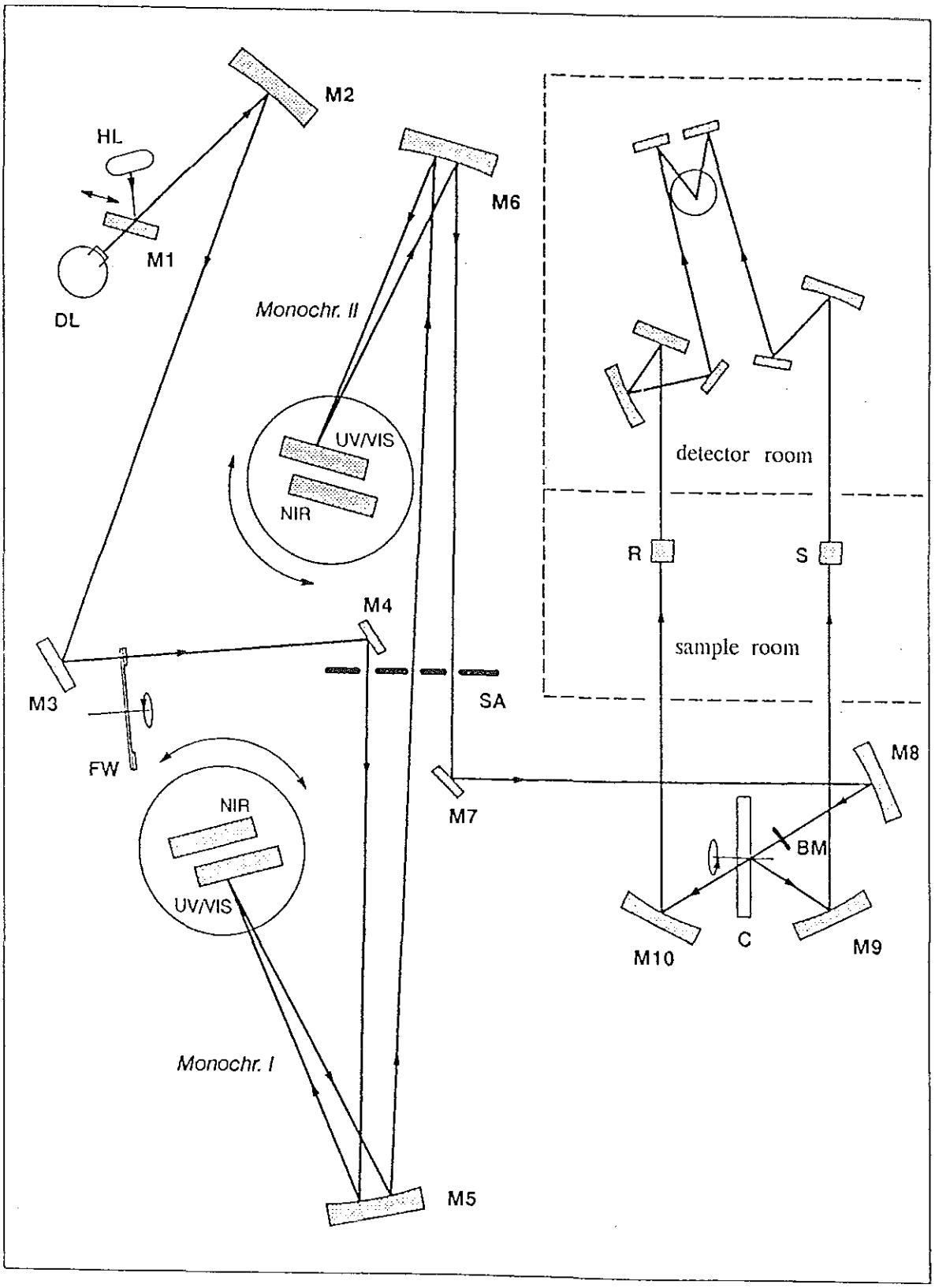

Fig. 3.1 Optics of Lambda 19 spectrophotometer

Description of Fig. 3.1:

- DL is Deuterium lamp that produces UV light
- HL is Halogen lamp that produces VIS/NIR light
- M1 stands for mirror number 1
- FW stands for Filter Wheel that filters light from the source
- SA is a slit
- Monochr. is an abbreviation for monochromator
- C is a chopper (half hole and half mirror disk) that divides the single beam into two
- BM stands for Beam Mask
- In the sample room there are two ports where R (reference mirror holder) and S (sample holder) can be installed.
- And at last, the detector compartment comes were two type of detectors exist. PMT (photo multiplier tube) that detects UV/VIS light and PbS (Lead sulfide semi-conductor) detector that detects NIR light

3.2 Experimental procedures

Spectrophotometer measures the ratio of intensity of the sample reference beam. Before measuring samples it is necessary to perform an in correction.

3.2.1 Near normal incidence R and T measurements

To measure near normal incidence R and T Lambda 19 spectroph compartment was used and measurements have been performed as follow

a/ reflectance (R) measurement

i. The spectrophotometer was switched on and waited for 20 minutes u thermal equilibrium.

ii. Using the software the appropriate scan method was chosen.

iii. Reference and sample beam reflectance holders were mounted in normal compartment. After putting standard mirrors on both holders background correction (BC) was done. The machine automatically re is the ratio of the intensity of sample beam (I_s) to intensity of refer

$$BC = I_s/I_r$$

iv. The mirror on the sample beam was replaced by a sample to be me measurement was performed. The ratio Fr,

$$Fr = (I_s*R)/(I_r*R_r) = BC*(R/R_r)$$

where R is reflectance of the sample

and R_r is the reflectance of the standard

was measured by the machine and the ratio Fr/BC was displayed on

v. To obtain the reflectance of the sample the displayed result was mu calibration data (R_r).

$$R = (Fr/BC)*R_r$$

b/ transmittance (T) measurement

i. Both reflectance sample holders were taken out of the normal compartment and transmittance sample holder was installed in the sample beam.

ii. Instrument background correction (BC) was performed.

iii. The sample was installed on the transmittance holder and measurement was performed. The displayed result is

$$T = Fr/BC.$$

c/ The absorption coefficient (α) of the sample was calculated using the program we have prepared in HTBasic software (appendix) and the relation of eqn. (2.3.3) from the measured values R and T. The data for Tauc's plot was also calculated using our pro gram.

d/ The optical gap E_g was determined using Tauc's plot, i.e. from the plot of sqrt($\alpha h\nu$) vs $h\nu$.

e/ Dielectric functions (ϵ_1, ϵ_2), refractive index (n), extinction coefficient (κ) as a function of wavelength and thickness of the sample were simulated from R_p and R_s results. For simulation, W.V.A.S.E. (variable angle spectroscopic ellipsometer software for windows) was used.

3.2.2 Angle resolved reflectance measurements

i. Spectrophotometer was switched on and waited for 20 minutes till lamps reach thermal equilibrium.

ii. Using the software the appropriate scan method was chosen.

iii. Polarizer's were fixed on reference and sample beams.

iv. Variable angle reference and sample reflectance holders were mounted in normal compartment. After putting standard mirrors on both holders and setting angle, instrument background correction (BC) was done.

The machine automatically recorded BC, that is the ratio of the intensity of sample

beam (I_s) to the intensity of reference beam (I_r)

$$BC = I_s/I_r$$

v. The mirror on the sample beam was replaced by a sample to be measured and the measurement was performed. The ratio Fr,

$$Fr = (I_s*R)/(I_r*R_r) = BC*(R/R_r)$$

where R is reflectance of the sample

and R_r is the reflectance of the standard.

was measured by the machine and the ratio Fr/BC was displayed on the screen. In our case, R_r was simulated from ellipsometer data.

vi. To obtain the reflectance of the sample the displayed result was multiplied by the calibration data (R_r).

$$R = (Fr/BC)*R_r$$

vii. Dielectric functions (ϵ_1,ϵ_2), refractive index (n), extinction coefficient (κ) as a function of wavelength and thickness of the sample were simulated from R_p and R_s results. For simulation, W.V.A.S.E. (variable angle spectroscopic ellipsometer software for windows) was used.

3.2.3 Integrating sphere

In principle integrating sphere (RSA-PE-90), Fig. 3.2, is the same as the normal compartment except the integrating sphere measures also the scattered light. Because it collects diffused light, it is also known as diffuse reflectance and transmittance accessory. The internal part of the sphere is made up of white material that diffuses light in all directions. The standard reflectance material or SRS-99 reference material (spectralon) and light trap were used. SRS-99 is made up of white material that diffuses light falling upon it to nearly 100% in the whole spectral range. The integrating sphere has sample mounting ports for reflectance and transmittance measurements, and a reference port for standard material. It also provides a center mount sample holder that allows R and T measurements at different angles. BC and Fr are defined as for normal compartment and the quantities that the machine measures are also the same.

i. Spectrophotometer was put off and dismounted from the power supply.

ii. The detectors of normal compartment were disconnected and normal compartment was replaced by integrating sphere. Integrating sphere detectors were connected.

iii. Switching on the machine for 20 minutes, spectralon was mounted either on wall mount or on center mount and BC was done.

iv. For reflectance measurements, the standard reference material was replaced by a sample and measurement was performed. The ratio Fr/BC was displayed.

v. To get R of the sample the result of step iv. was corrected by the reflectance data of the reference material.

vi. For transmittance measurements the sample was mounted on the transmittance port and the measurement was performed. All transmitted light was measured and T was displayed.

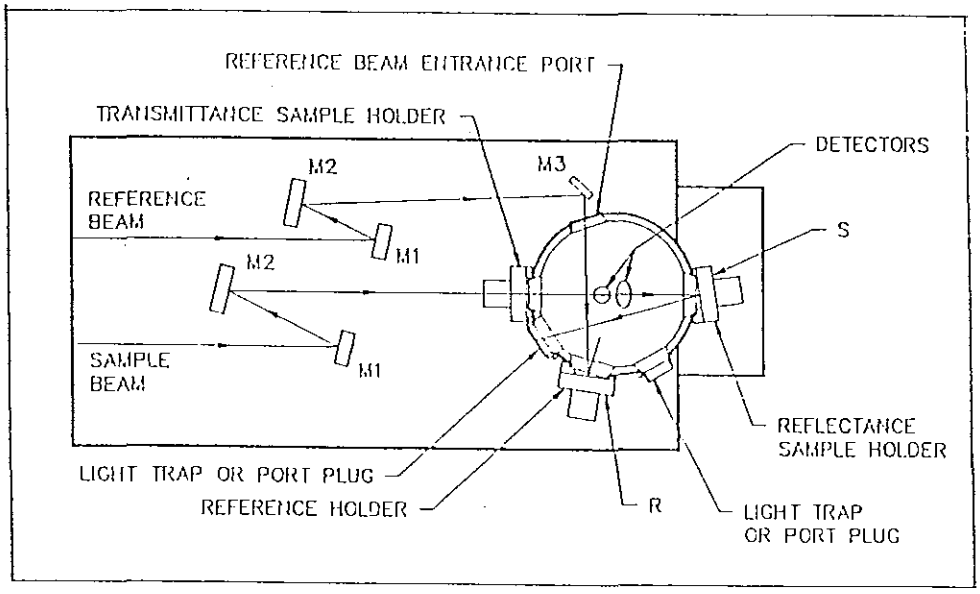

Fig. 3.2 Optics of integrating sphere

4. RESULTS AND DISCUSSION

4.1 p-i-n solar cell structure

Photovoltaic (solar cells) convert the sun light directly into electricity. The energy converted by solar cells is renewable and friendly to our environment. Solar cells can be produced from different materials. Crystalline silicon, GaAs, and a-Si:H and its alloys are among the materials from which solar cells can be produced. However, a-Si:H and its alloys thin film technology show a promising new approach for low cost solar cells development.

There are different solar cell structures of a-Si:H and its alloys thin film. These structures include p-i-n, p-i-n-p-i-n (tandem solar cell), and Schottky-barrier cell. Each structure has its own advantage and disadvantage. For instance, depositing p-i-n solar cells is more simple and requires much less time than p-i-n-p-i-n solar cells. Where as p-i-n-p-i-n solar cells have the ability to absorb light in wider wave length range. When light falls on the p-i-n-p-i-n solar cells, energetic light that do not absorb on the front p-i-n layers have the opportunity to be absorbed in the next p-i-n layers. The back p-i-n is prepared in such a way that it will absorb the light that passes through the front p-i-n layers. Thus, p-i-n-p-i-n cells using their two p-i-n layers can absorb more than p-i-n solar cells. Of course p-i-n solar cells have also the ability to absorb much of the light in the wave length range where the light intensity is strong. Among these structures, we have characterized p-i-n solar cell and each layers. Here (Fig. 4.1) is a schematic structure of a-Si:H p-i-n solar cell.

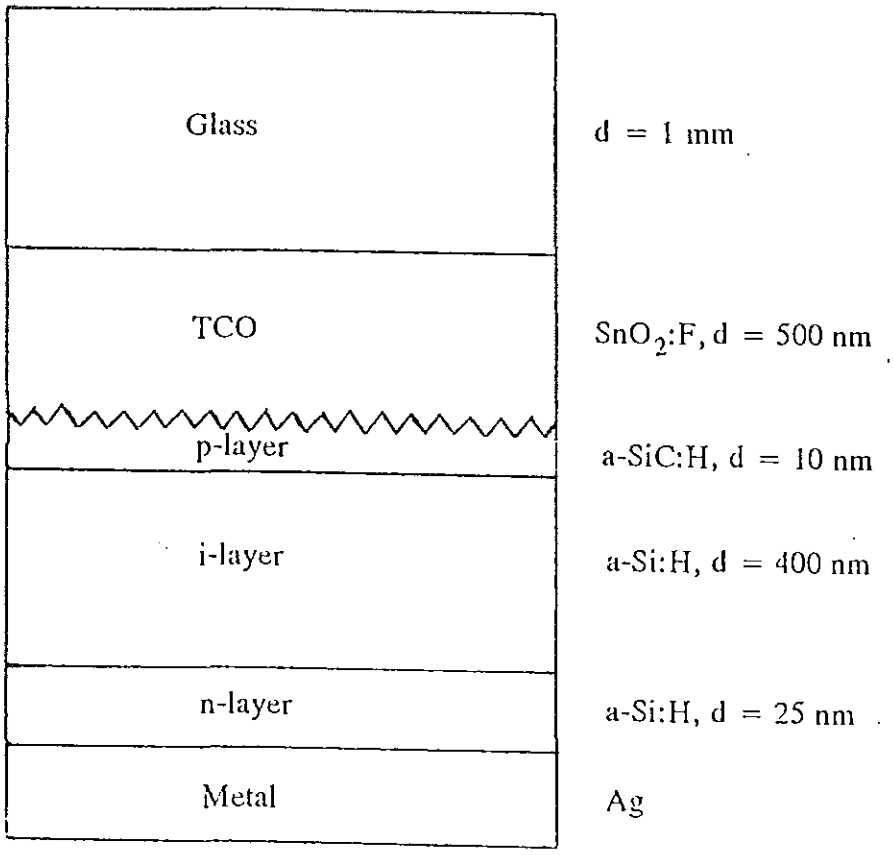

Fig. 4.1 p-i-n solar cell structure

Fig. 4.1 is a schematic cell structure and the thickness of each layer is a typical value. In the next section, the use of each layer in the solar cell from their optical characteristic point of view will be considered.

4.2 R, T and α of layers

4.2.1 Transparent conducting oxides (TCOs)

Transparent conducting oxides in solar cells play an important role. One of the primary roles of TCO in solar cell is that it serves as a front ohmic contact for the solar cell. Moreover, TCO is scattering the light passing through it. Scattering enhances long wavelength light absorption by increasing optical path length of the incident light [7,22,23]. The TCOs used for our experiments are fluorine doped (SnO_2:F).

For the discussion of the nature of TCOs and absorption of light in layers, understanding of the radiation spectrum is necessary. So, let us discuss a little about radiation.

The black body is a physical model for a body that absorbs all the radiant energy incident upon it regardless of wavelength [15]. It is clear that if the body is in equilibrium with its surrounding, it emits as much energy as it absorbs. Planck asserted that an atomic resonator could absorb or emit only discrete amount of energy which is compatible with its oscillatory frequency. Moreover, he asserted that each such an energy value is an integral multiple of $h\nu$. i.e.

Energy (E) = $mh\nu$

where h stands for Planck's constant, h = $6.626*10^{-34}$ Js.

and m is a positive integer.

He also derived a relation (eqn. (4.1)) for spectral excitance (I_s). He arrived at this relation by fitting curves to the experimental data.

$$I_s(\lambda) = \frac{2\pi hc^2}{\lambda^5}\left[\frac{1}{e^{\frac{hc}{\lambda kT}} - 1}\right] \qquad (4.1)$$

where speed of light (c) = $3*10^8$ m/s,

and Boltzmann constant (k) = $1.381*10^{-23}$ J/K.

The scattering ability of TCO depends on how rough the TCO is. Haze is defined by eqn.(4.2) and eqn.(4.3). We have determined haze of rough, standard and flat TCOs. The TCOs measured have the following thicknesses: d = 90 nm (flat TCO), d = 500 nm (standard TCO), and d = 800 nm (rough TCO).

Haze of TCO is often measured with "white" light, i.e. a standard 5400 K black body source. For the "natural" haze one would have to multiply the spectral dependent haze with AM 1.5 solar spectrum. For evaluation of laboratory measurements a standard 5400 K black body source is often used. In our case too, intensity of light from 5400 K black body source on the surface of the earth (Fig. 4.2) was used to find haze of our TCOs. I_s for a standard 5400 K source was calculated using eqn. 4.1 and converted to I_e (intensity of sun radiation on the surface of the earth) by taking the distance between the sun and the earth into consideration. The relation between I_s and I_e is: $I_e = (r_s/r_e)^2 * I_s$, where $r_s = 7*10^5$ km is radius of the sun and $r_e = 1.5*10^8$ km is the distance between earth and sun. Spectrum of I_e is a smooth curve but AM 1.5 spectrum [26] has some minima which arise due to light absorption by H_2O, CO_2 and other molecules in the air .

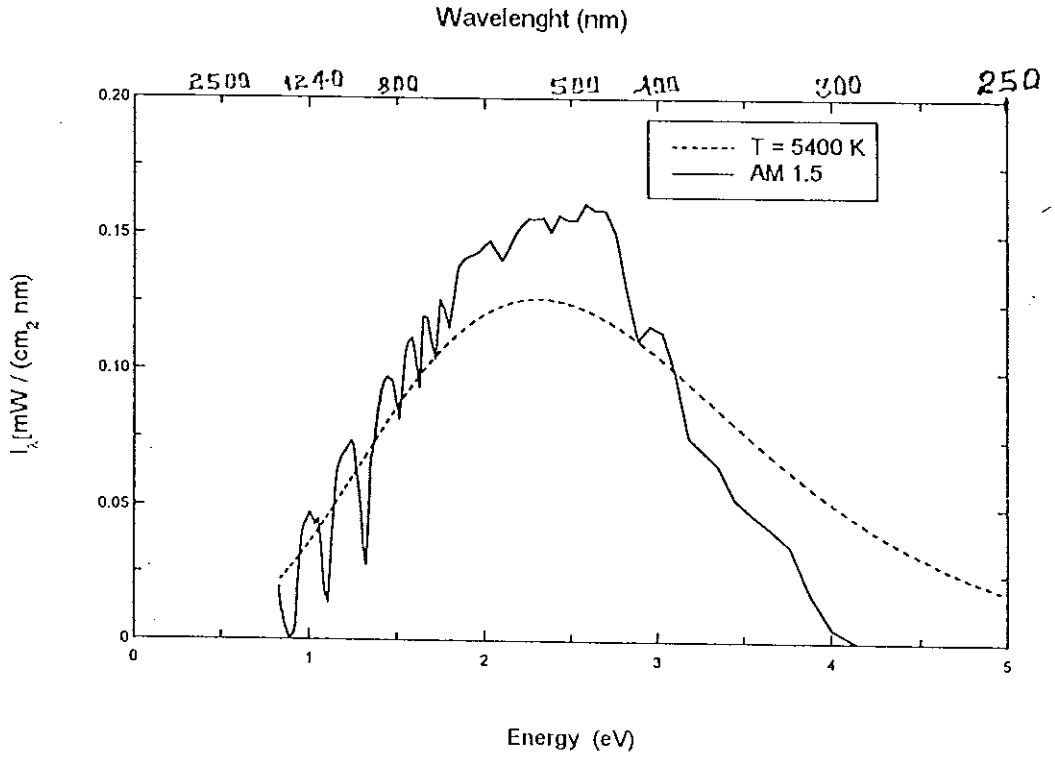

Fig. 4.2 AM 1.5 - spectrum and black body radaition at T = 5400 K

The sun radiation spectrum (fig. 4.2) has maximum spectral irradiance at around 500 nm. Wien's law, $T^*\lambda_{max} = 2.8978^*10^{-3}$ mK asserts that for T = 5400 K the maximum spectral irradiance occurs at λ_{max} = 536 nm. Thus, for maximum output, the solar cells must be designed in such a way that they absorb much of solar energy around 500 nm. That is the region of interest where solar cells should absorb much.

The spectral haze (H) is defined as the ratio of the difference between total transmittance (T_t) and specular transmittance (T_s) to T_t, i.e.

$$H_s(\lambda) = \frac{T_t - T_s}{T_t} \qquad (4.2)$$

And the total haze (H_T) is determined from H_s using eqn. (4.3).

$$H_T = \frac{\int I_e(\lambda,5400K)\,H_s(\lambda)\,d\lambda}{\int I_e(\lambda,5400K)\,d\lambda} \qquad (4.3)$$

T_s was measured using the normal compartment while T_t was measured by collecting all transmitted light using the integrating sphere. The results are as given by Fig. 4.3 a, b and c.

a) rough TCO

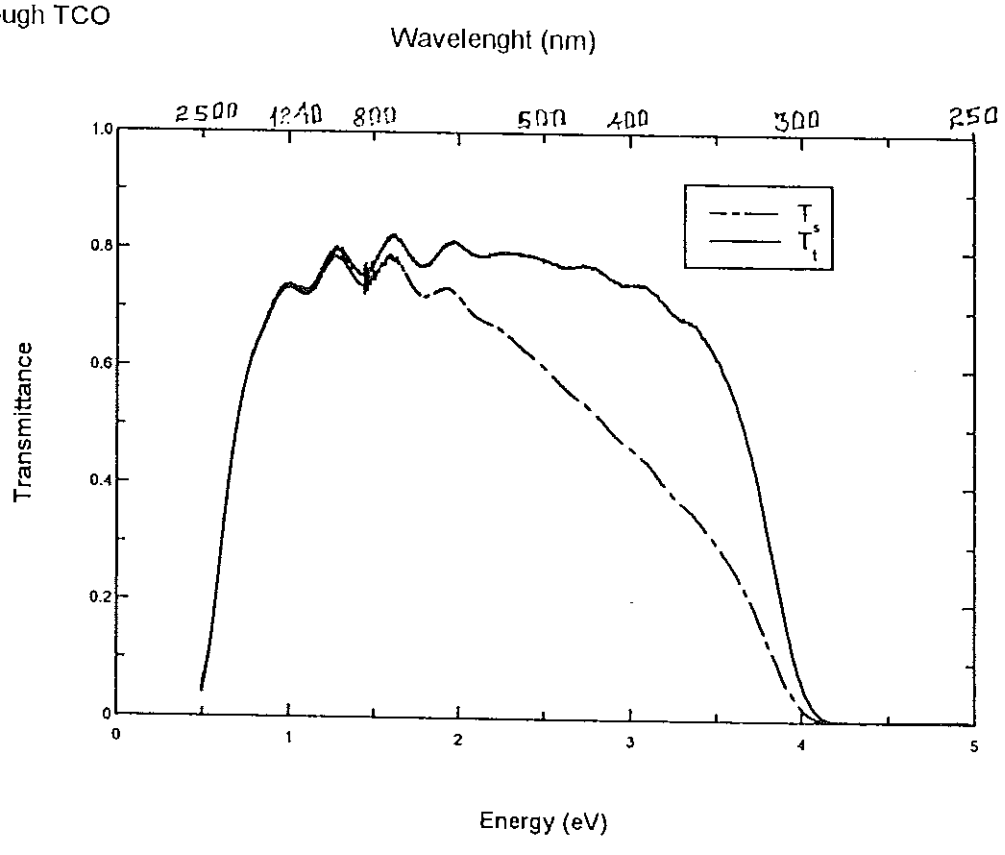

b) standard TCO

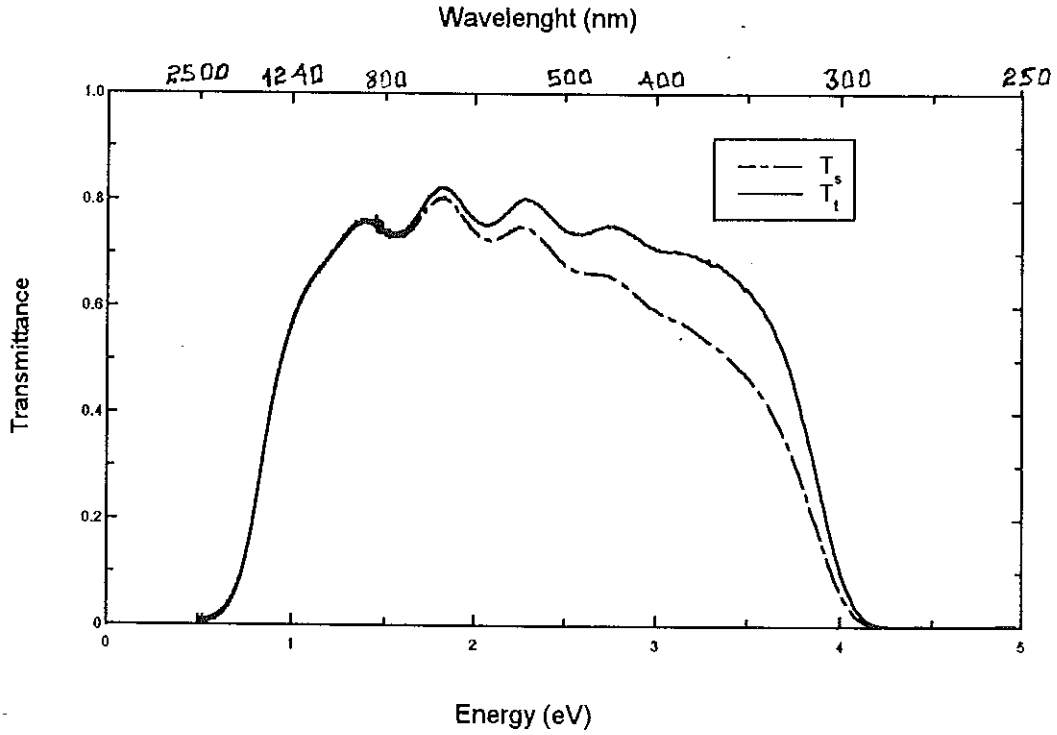

c) flat TCO

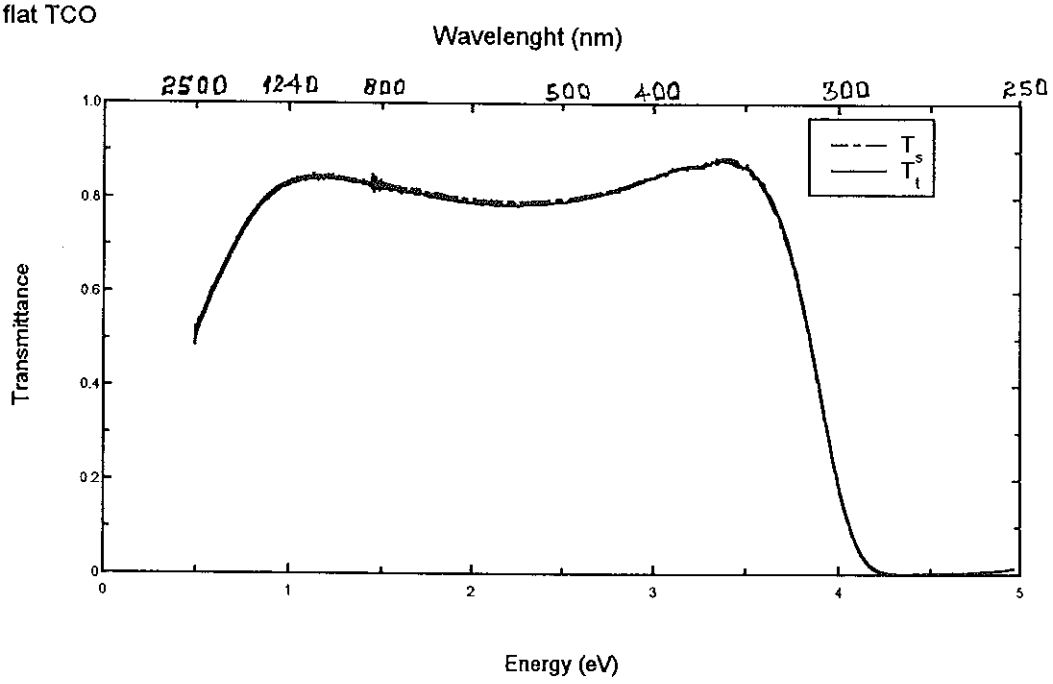

Fig. 4.3 Total and specular transmittance of a) rough, b) standard and c) flat TCOs.

The interference fringes we observe on the spectrum of T of the standard and rough TCOs are due to the thickness of the films. Thickness of the films, d = 500 nm for standard and d = 800 nm for rough TCOs are comparable with the wavelengths where the fringes are observed. But in the case of flat TCO a thickness of d = 90 nm is small. The interference fringe observed on the curve of flat TCO is broad. The fine interference fringes lie outside of measured wavelength range.

For higher wavelength (lower frequency) the transmittance of TCOs drop exponentially [15]. The reason, why the transmittance of TCOs drop exponentially, is that TCOs act as a metal. Metals have complex refractive indices [15,16]. It is clear that if refractive index is complex the incident disturbance will be attenuated exponentially and thus much of the incident intensity will be absorbed.

Since rough and standard TCOs scatter much of the incident intensity around 500 nm, the total transmittance is greater than the specular transmittance (Fig. 4.3), while the total and the spectral transmittance of flat TCO are nearly the same. Thus from figure 4.3 one observes that the rough TCO scatters more than the standard TCO, whereas the standard TCO scatters more than the flat TCO. The difference between the total and specular transmittance describes also that the rough TCO scatters most.

The spectral haze of the rough TCO is greater than that of the others (Fig. 4.4), indicating once again that the rough TCO is the most scattering TCO. Fig. 4.4 of the spectral haze indicates also that standard TCO scatters more than flat TCO.

Above 1000 nm, the transmittance of rough TCO is greater than that of standard TCO. This indicates that standard TCO exhibits more metallic properties than rough TCO.
By the same argument, flat TCO exhibits less metallic properties than the others for wavelengths greater than 1000 nm.

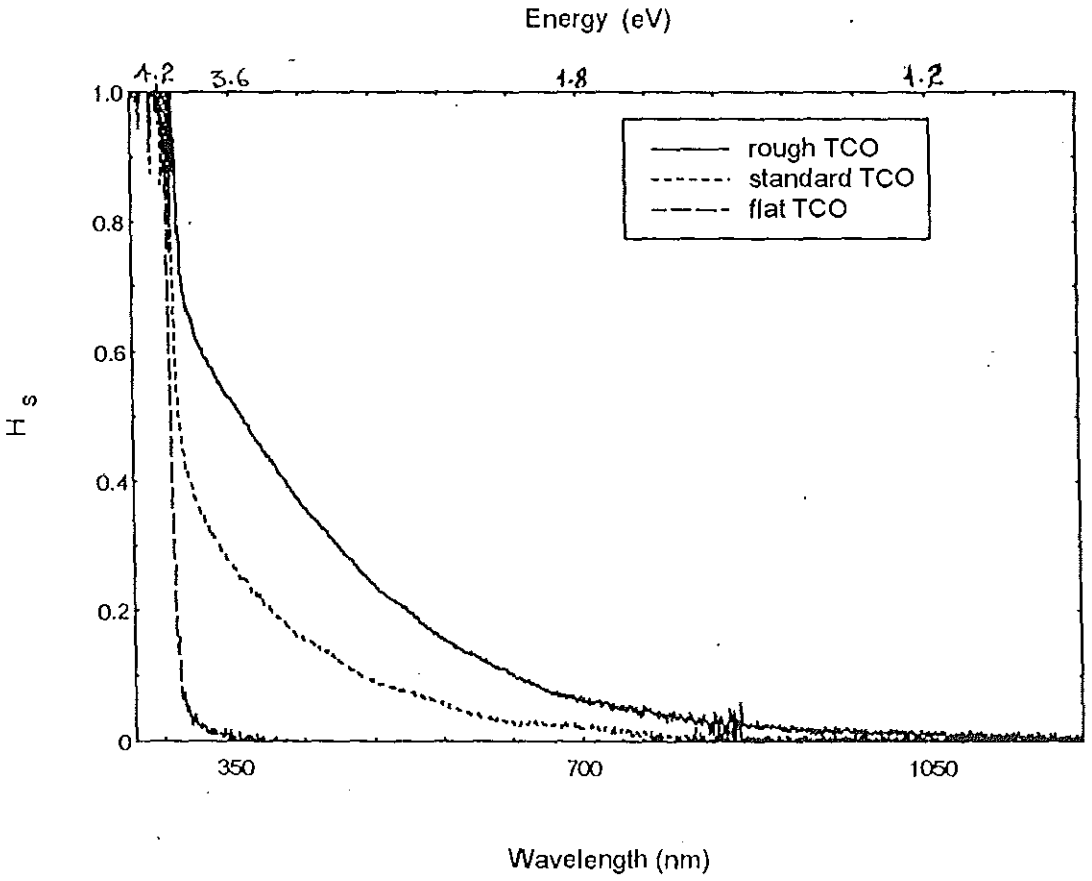

Fig. 4.4 Spectral haze of different TCOs.

The values of total haze calculated with eqn. 4.3 is found to be 0.95%, 7.7% and 13% for flat, standard and rough TCOs respectively. The values of total haze 0.3% and 22% for flat and rough TCOs respectively was given by the manufacturer. The total haze we have determined for the TCOs also prove that rough TCO is the most scattering TCO.

From optical characteristic point of view, because of its high scattering ability, using rough TCO in the solar cells is more advantageous. But, the rough TCO is not as metallic as the standard one above 1000 nm.

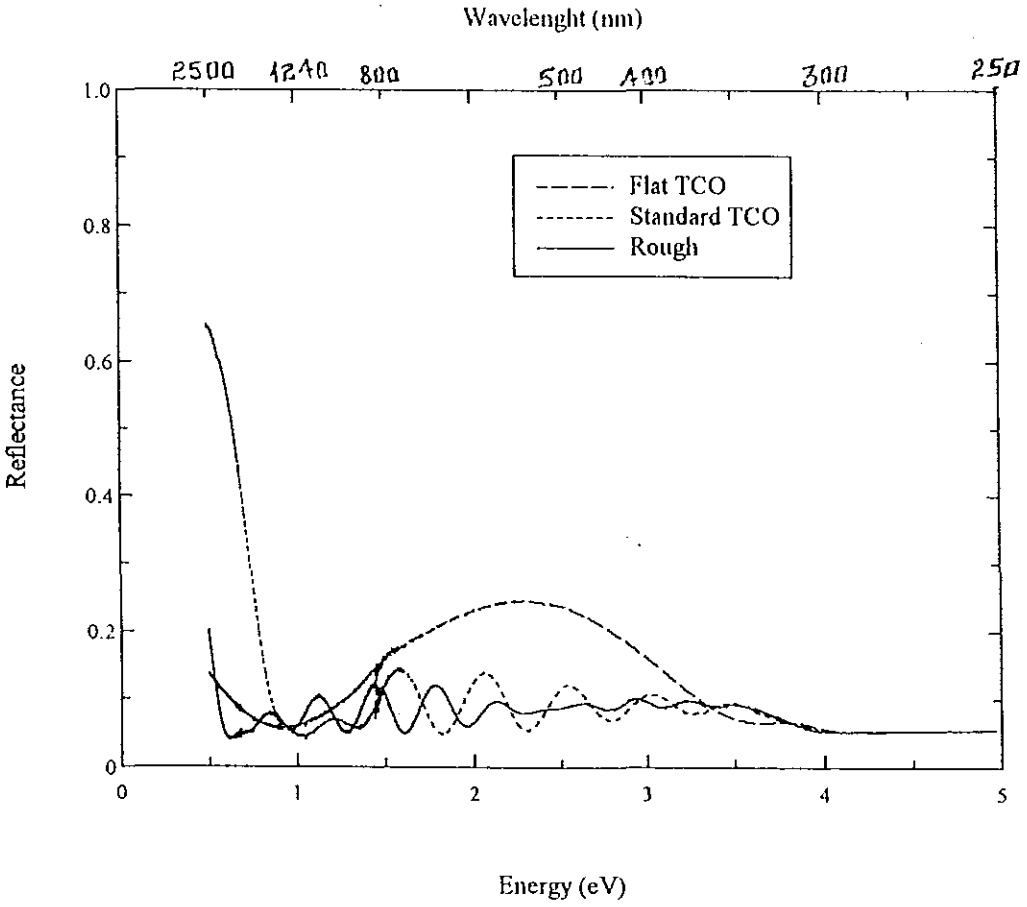

Fig. 4.5 Specular reflectance of different TCOs.

All reflectance and transmittance measurements of TCOs are carried out in such a way that light enters from the glass side. i.e. light-glass-TCO.

The reflectance of flat TCO around 500 nm is much pronounced than that of the others (Fig. 4.5). For this reason using flat TCO in solar cells is disadvantageous from optical point of view. However, the reflectance of the Asahi U TCO around 500 nm is smaller than that of the standard TCO. Therefore, from optical side, using Asahi U TCO is advantageous specially for wavelengths less than 1400 nm. But, above 1400 nm Asahi U reflects most and thus has poor metallic behavior.

4.2.2 p-, i-, and n- layers

In addition to the optical properties of the solar cells, design of hydrogenated amorphous silicon thin film solar cells require understanding of the optical properties of individual layers [4,5]. The method often chosen for characterizing a-Si:H and its alloys in the spectral range of fundamental absorption are from R and T measurements [1,15-18]. We have carried out R and T measurements of p-, i-, and n- layers using Lambda 19 spectrophotometer (Fig. 4.6 a, b and c) to study their optical properties. All the layers, which we have measured, have a thickness of approximately 1000 nm.

a/ p - layer (d=1000 nm)

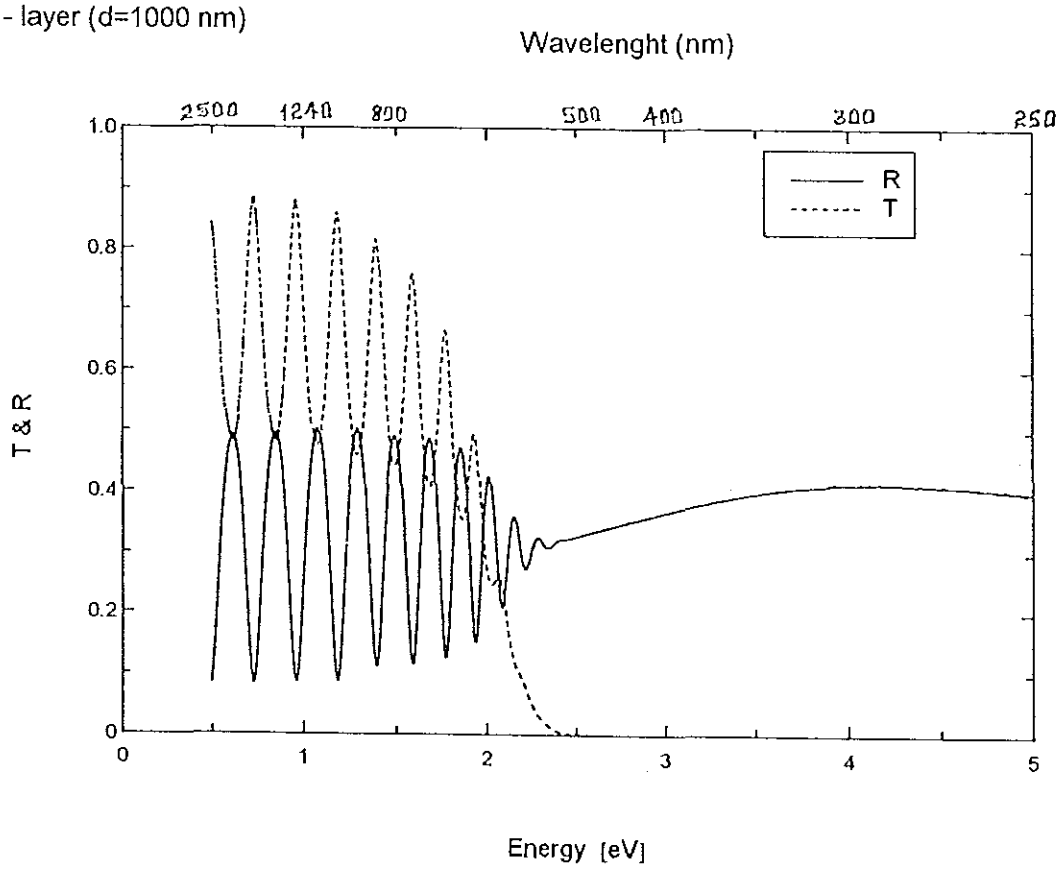

b/ i - layer (d=1005 nm)

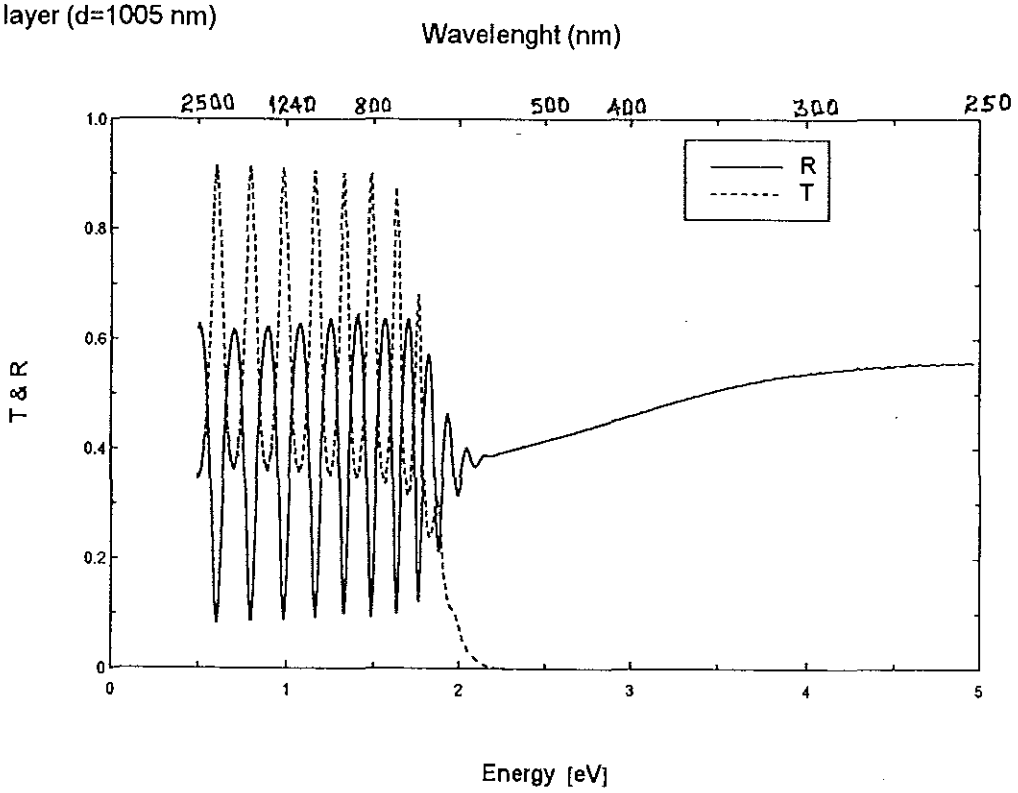

c/ n - layer (d=955 nm)

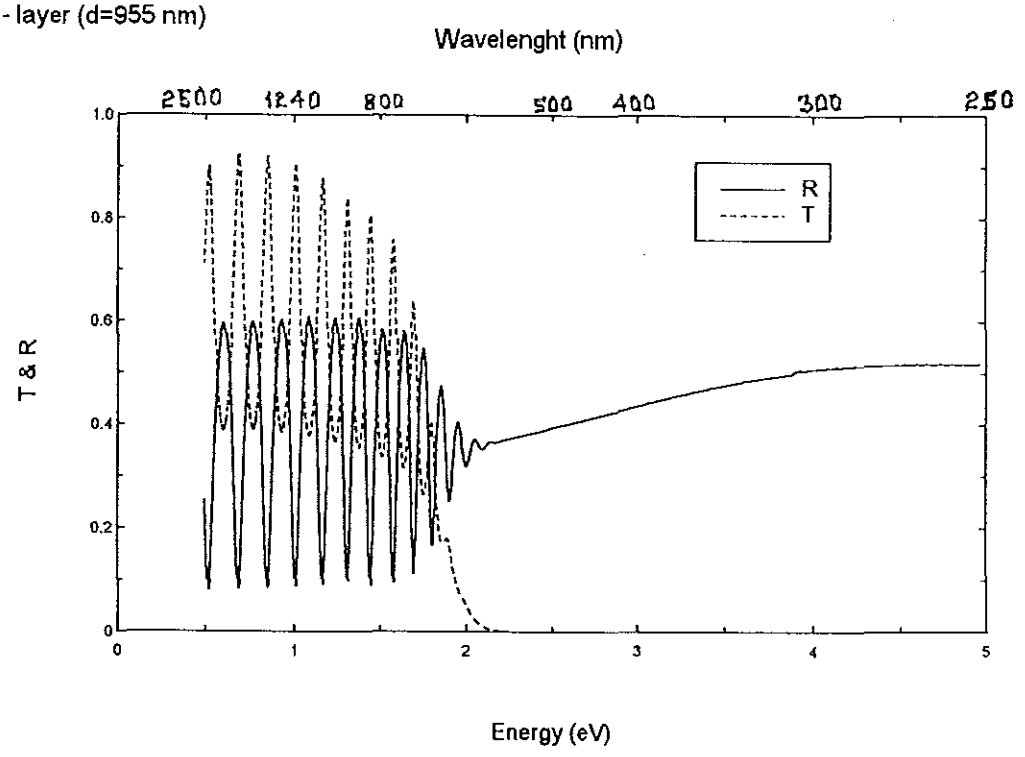

Fig. 4.6 R and T of a/ p, b/ i, and c/ n - layers

The spectral fringes on R and T curves of Fig. 4.6 are due to the thickness of the films. The periodicity of the fringes are inversely proportional to the product of the thickness and the refractive index of the film. Obviously, the thicknesses of the films do not change with increasing wavelength. However, the refractive indices of the films are energy dependent. At lower energies, since the refractive indices of the films are decreasing with decreasing energy, the spectral fringes on the curves of R and T measurements are getting broader with decreasing energy .

The reflectance curves of all layers above 2.2 eV energy show a tendency to increase, whereas the transmittance curves do not show a significant change. Transmittance is strongly connected with penetration depth. The penetration depth of an absorbing material is equal to an inverse of the absorption coefficient [15,16]. Thus, since amorphous materials have high absorption coefficient, the transmittances of the layers above 2.2 Ev are negligibly small to be detected by spectrophotometer.

For energy range between 1.5 and 2.2 Ev, the amplitude of the spectral fringes on R and T curves are not equal (Fig. 4.6) because of the absorption of light in the layers. This is the range where hydrogenated amorphous silicon thin films have a very high absorption coefficient.

We note from the tail of the transmittance curves (Fig. 4.6) that p-layer stops transmitting at relatively higher energies. Thus, p-layer has more band-pass which allows much light to pass through.

From the magnitude of the reflectance curves, we note also that the reflectance of the p-layer is small as compared to the reflectance of i- and n- layers.

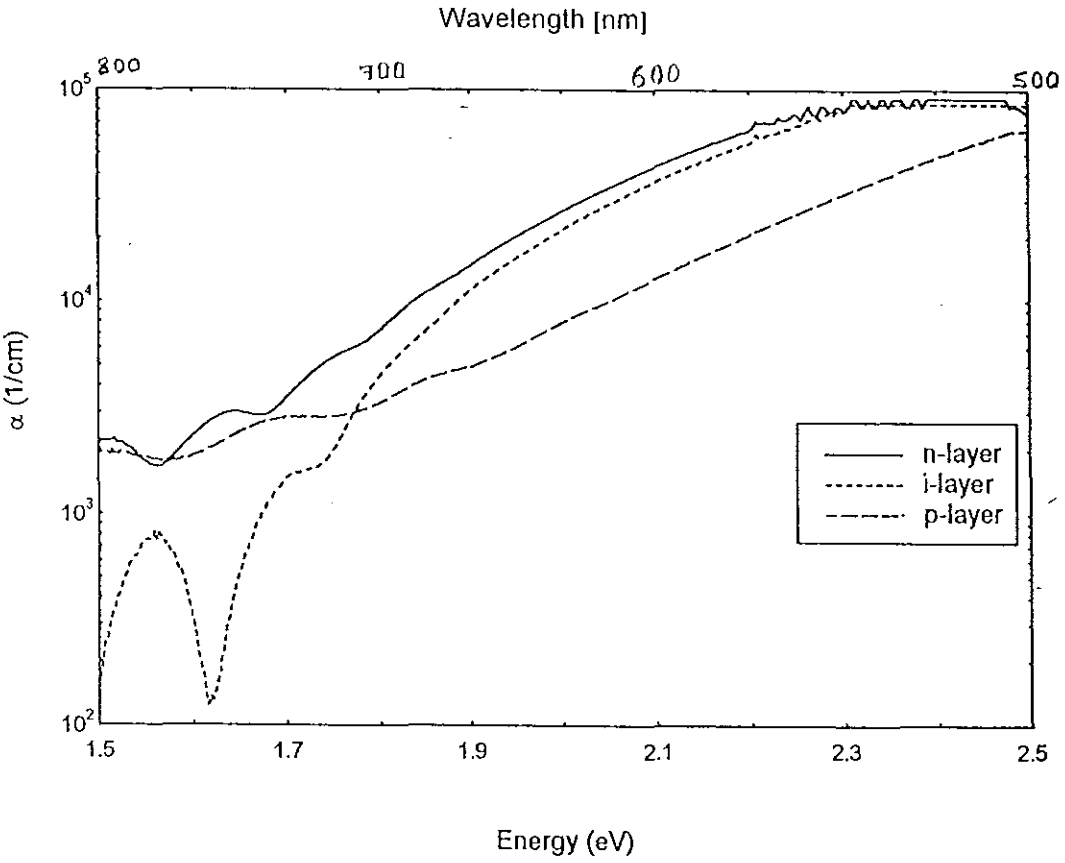

Fig. 4.7 Absorption coefficient of p-, i- and n- layers.

Fig. 4.7 contains information about the absorption coefficient of the layers we have considered. Information about the absorption coefficient of layers are crucial to optimize the structure of the solar cells in order to maximize light absorption in the active layer [22,23].

Between 1.75 and 2.5 eV, Fig. 4.7 shows that p-layer has low absorption coefficient which enables much light to pass into the i-layer without much absorption.

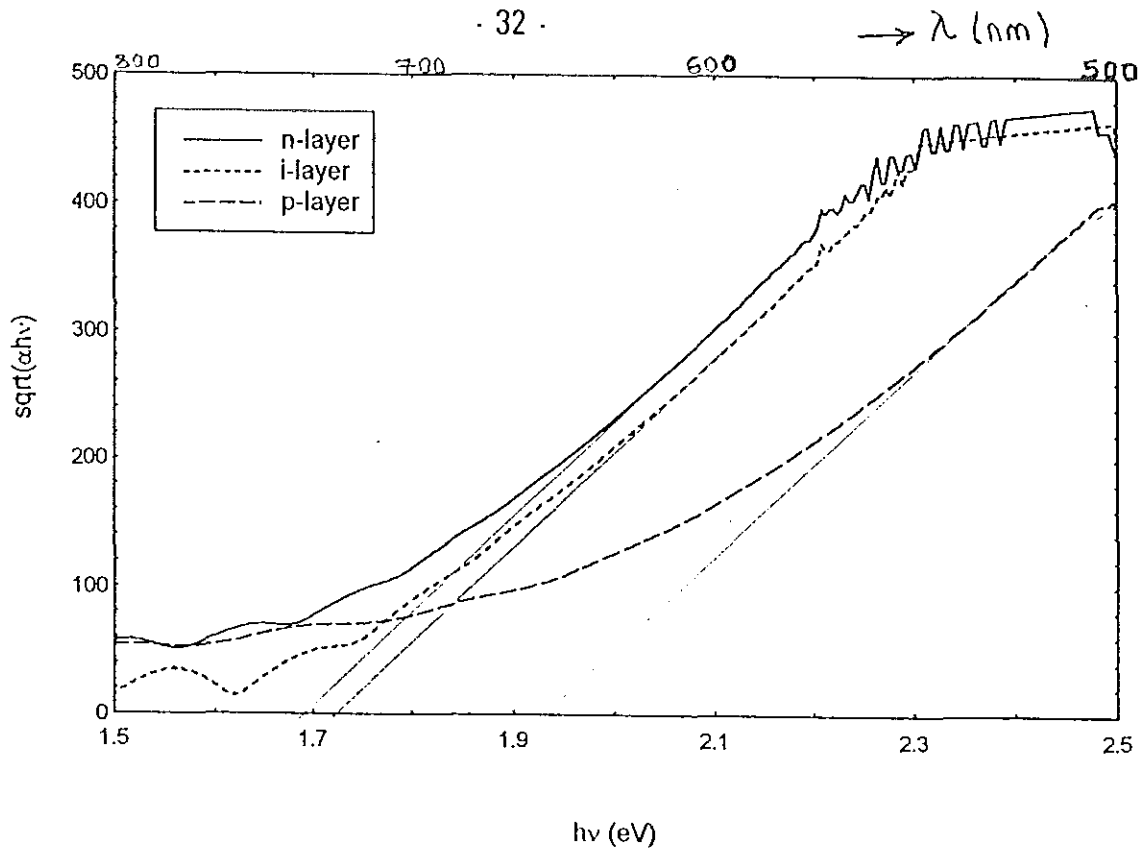

Fig. 4.8 Tauc's plot of p-, i- and n- layers.

The band gap of layers has a significant importance in the design of a-Si:H thin films solar cells because it affects both the short-circuit current and open-circuit voltage [7]. From Fig. 4.8, we observe E_g of n-layer (1.70 eV) is about the same or slightly smaller then E_g of the i-layer (1.72 eV). From transmittance and reflectance curves one can observe that i- and n- layers have similar optical properties in VIS light range. The p-layer we have measured has an E_g of 1.92 eV. This shows that much of VIS light (with energy less than 1.92 eV) can pass through the p-layer into the i-layer where it is needed to be absorbed.

4.2.3 Dielectric function of n-layer

The dielectric function of the n-layer is simulated using window version simulation software for variable angle spectroscopic ellipsometer (W.V.A.S.E.) from near normal incidence R-measurement (Fig. 4.9). For energies less than 1.5 Ev, ϵ_2 is zero. According to equation (2.4.1) ϵ_2 zero implies that either both n and K are zero or one of them is zero. Obviously n of a material is different from zero. It must be K which is zero. Thus, since K is directly proportional to α, n-layer has zero α for energies below 1.5 Ev. For the reason that n increases with increasing energy, ϵ_1 increases with energy even when ϵ_2 is 0. Above 1.5 Ev, both ϵ_1 and ϵ_2 are increasing because n and K are increasing.

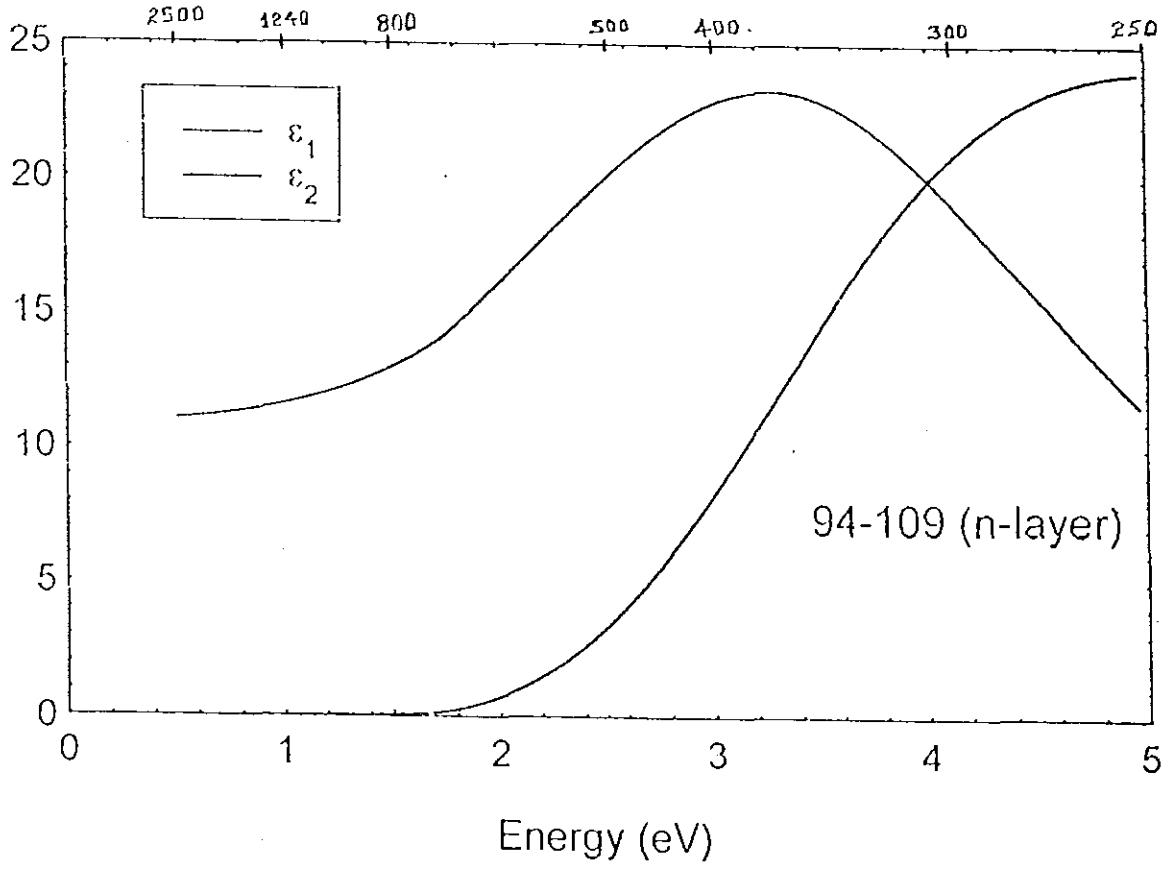

Fig. 4.9 Dielectric function of n-layer obtained form near normal incidence R measurement.

It is necessary to generate T curve from the obtained dielectric function and compare it with the near normal incidence T measurement . This comparison is important to prove whether the obtained dielectric function exactly describes the n-layer or not. The comparison (Fig. 4.10) shows that the fitted curve is almost the same with the measured T spectrum. This proves that determination of the dielectric function of layers by near normal R and T measurement method is a precise way except for non-transparent materials. T measurement is impossible for non-transparent materials. So if you want to determine dielectric function of non-transparent by this method, you can not counter check the obtained result. In this case, it is possible perform R_s and R_p measurements and determine dielectric function therefrom.

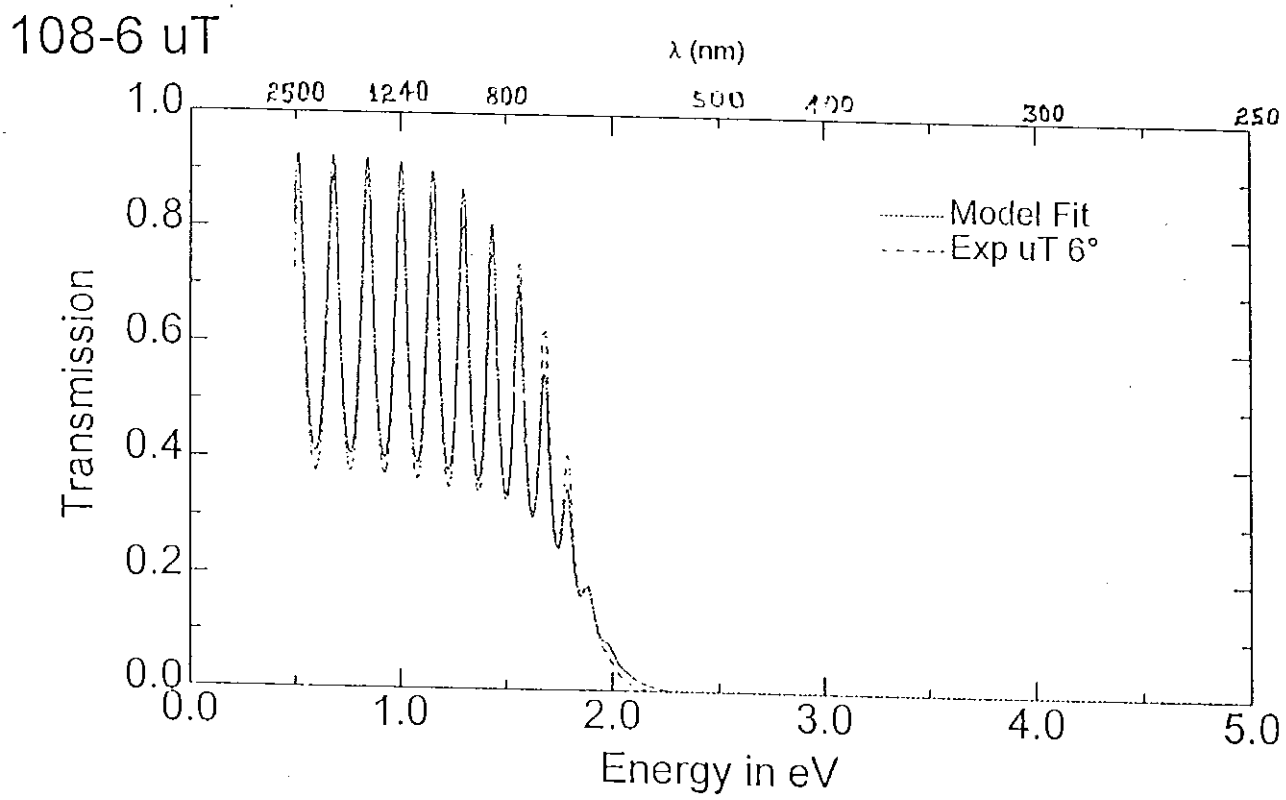

Fig. 4.10 Measured and fitted transmittance of n-layer.

4.2.4 R_s and R_p measurements

First, R_s and R_p (fig. (4.11)) of the corning glass have been measured. While performing R_s and R_p measurements of the corning glass, we have fixed a prism from the back of the sample using index matching fluid to avoid light reflected from the back surface. That is to avoid the light reflected from the glass-air interface. Except for higher angles (specially above 60°) where the measurement is affected by false light which reflects from the frame of the holder, the experimental curves are in good agreement with the fitted curve. This result gives information how exact our R_s and R_p measurements using the spectrophotometer is.

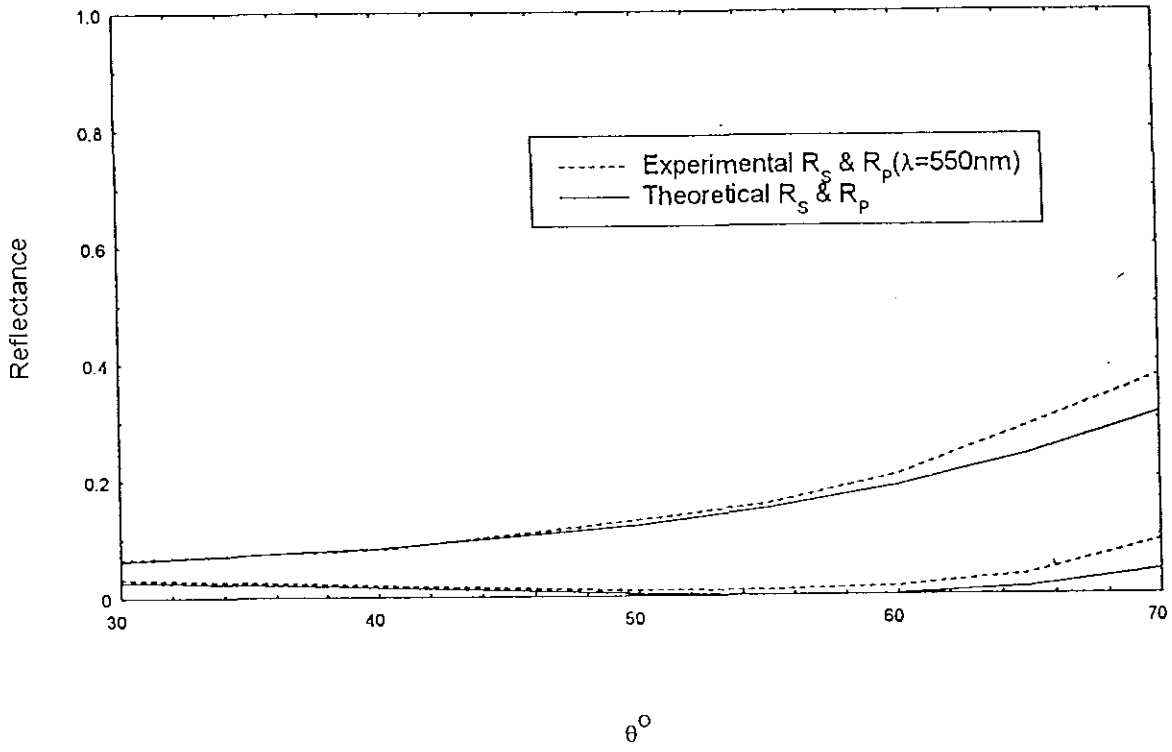

Fig. 4.11 Measured and fitted R_s and R_p of mirror.

And then, R_s and R_p measurements at 60° for different layers was performed. The measured R_s and R_p curves together with the fitting results are as shown fig. (4.12).

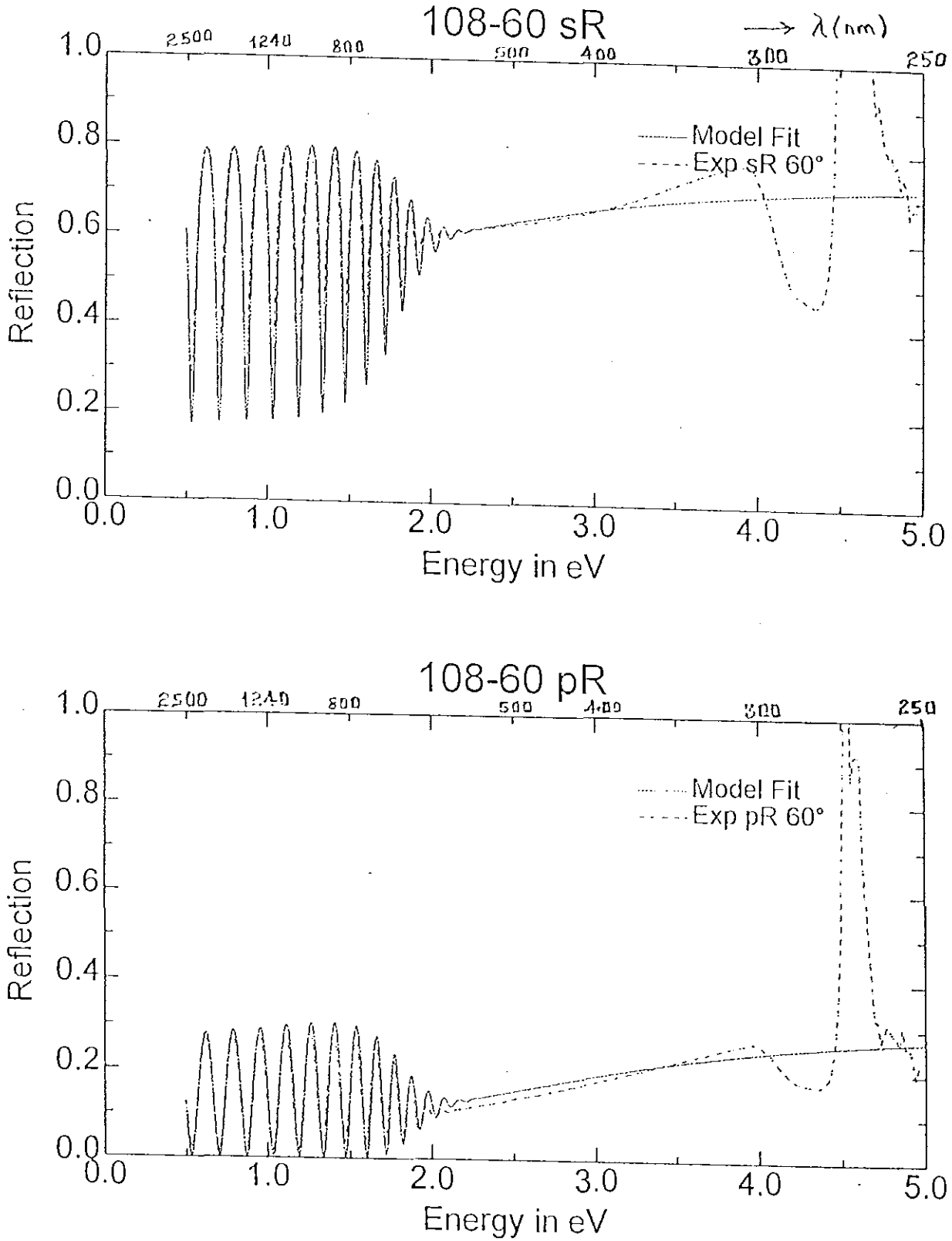

Fig. 4.12 Measured and fitted R_s and R_p n-layer.

R_s and R_p curves for incident angle 60° is generated by W.V.A.S.E from the dielectric function which was obtained from near normal R measurement. The generated curves are compared with the result of 60° incidence angle R_s and R_p measurement.

Unexpected behavior is observed on the measured spectrum of R_s and R_p of layers for energy above 3 Ev. It is so because of the index matching used at the back. At higher energies the index matching fluid used starts to reflect. Even at some energies it reflects nearly 100%. In the remaining energy range the measured R_s and R_p curves are in agreement with the fitting result. The small deviation observed can be accounted by false light reflected from the frame of the holder. It is possible to improve R_s and R_p measurements for determination of the optical constants of absorbing thin films on a substrate by reducing the effect of the reflected false light. Of course, even with the existence of false light, R_s and R_p measurements we have done is not bad. It fairly fits to the curve generated from dielectric function which obtained from near normal incidence angle R measurements.

The advantage of using this method is that it helps to determine the optical constant of non-transparent materials. That is with out T measurement, one can determine the dielectric function of non-transparent films to the accuracy of 1%. The determination of optical constants from R_s and R_p measurements holds true also for transparent material with out performing T measurements.

The other advantage is that one can proof whether R_s and R_p measurements performed exact or not using relations; $R_{\parallel}$ (p-polarized light) and $R_{\perp}$ (s-polarized light).

4.3 Characterization of p-i-n a-Si:H solar call

The reflectance measurement of a-Si:H p-i-n complete solar cell is performed and simulated using W.V.A.S.E. to obtain the exact thickness of each layers (Fig. 4.13).

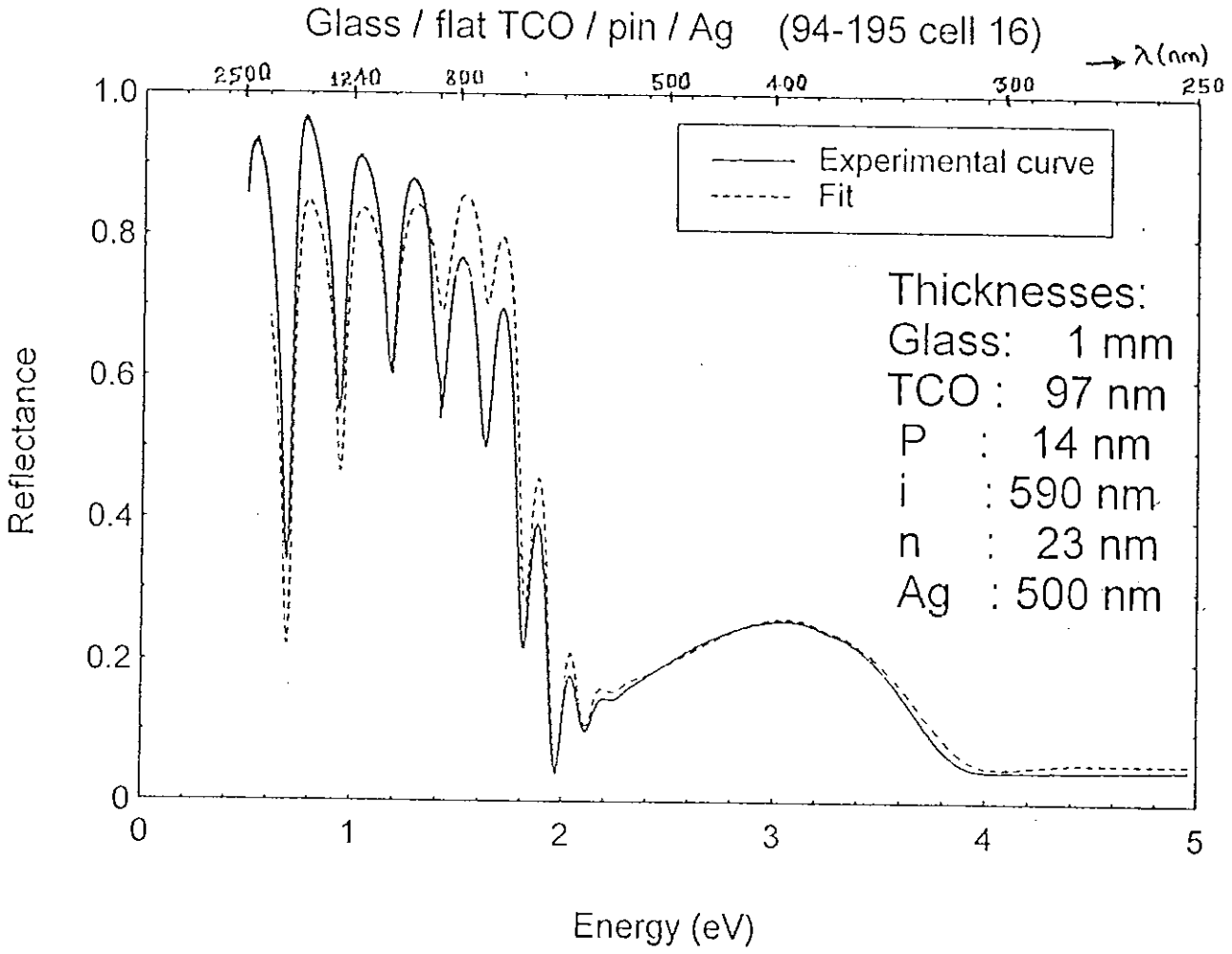

Fig. 4.13 R of a-Si:H p-i-n solar cell

The interference fringes on the curve over the intire range is dependent on the thickness of the reflecting layers. The broadness of the interference fringe is inversily proportional to the thickness of the layer from which light is reflected.

5. CONCLUSION

For the characterization of a-Si:H thin films, R and T measurements have been performed.

TCO in p-i-n a-Si:H solar cells which acts as a front ohmic contact must be transparent so that light passes into the inner layers. Scattering property of TCO enhances a long wavelength light absorption by increasing optical path length. Thus, TCO used in solar cell must have good metallic, scattering and transparency properties. Even though rough TCO with total haze 13% scatters most, its application in solar cell is hindered by its poor metallic property. Flat TCO with total haze 0.3% (poor scattering property) and high metallic property is not the material of choice for solar cell application. However, standard TCO having optimum scattering (total haze 7.7%) and metallic properties and also being transparent is an appropriate material for solar cell application.

Fundamental absorption in a-Si-H thin films occurs in the spectral range between 1.5 and 2.2 eV. p-layer, being next to the TCO and having optical band gap E_g = 1.92 eV passes incident light of energy less than 1.92 eV to the i-layer (E_g = 1.72) without absorption. i-layer having high absorption coefficient, however, absorbs most of the light in spectral range of fundamental absorption. Of course, this is the layer where light is needed to be absorbed. n-layer with E_g = 1.70 eV has similar optical properties with i-layer.

Characterization of thin films from R_s & R_g measurements at an angle different from near incident angle is reliable. Specially, characterizing non-transparent films by R_s & R_g allows a counter check.

R of solar cell depends on the thicknesses of individual layers used. In particular between 1.5 and 2.2 eV, R of solar cell is dependent on the thickness of i-layer.

6. REFERENCES

[1] United Solar System corp. (UNI-SOLAR), "Announcement", Dr. Subhendu Guha, Tel. (313) 362-4170, Fax: 810/362-4442, (1993) USA

[2] R. Street, Hydrogenated amorphous silicon, (Cambridge University Press, Cambridge, 1991) 362-372

[3] F.R. Zhu and Jai Singh, J. Non-Cryst. Solids 152 (1993) 75-82

[4] F.R. Zhu and Jai Singh, IEEE Proceedings (1993) [4]

[5] Kekn Hoffman and Troy Glatfelter, 23rd IEEE PVSC Louisvile. May (1993)

[6] F.R. Zhu and Jai Singh, J. Non-Cryst. Solids 152 (1993) 75-82

[7] Y. Hishikawa, S. Okamoto, K. Wakisaka, H. Nakamura, S. Tsuda, S. Nakano, M. Ohnishi, and Y. Kuwano, EC PVSEC February (1985) 37-40

[8] D. A. Minkov, J. Appl. Phys. 22 (1989) 199-205

[9] M. B. Tzolov, N. V. Tzenov and D. I. Dimova-Malinovska, J. Appl. Phys. 26 (1993) 111-118

[10] S. Nitta, S. Itoh, M. Tanaka, T. Endo and A. Hatano, Solar Energy Materials 8 (1982) 249-257

[11] C. L. Nagendra, and G. K. M. Thutupalli, Vacuum 31 (1981) 141-145

[12] Y. Hishikawa, S. Okamoto, K. Wakisaka, H. Nakamura, S. Tsuda, S. Nakano, M. Ohnishi, and Y. Kuwano, Jpn. J. Appl. Phys. 30 (1991) 1008-1014

[13] R. Swanepoel, J. Sci. Instrum. 16 (1983) 1214-1221

[14] N. Maley, Jpn. J. Appl. Phys. 31 (1992) 768-769

[15] E. Heaht and A. Zajac, Optics, (Addison-Wesky Publishing Comp., New York, 1987) 94

[16] K. L. Chopra, Thin Film Phenomena, (McGraw-Hill Book Comp., New York, 1969) 723-793

[17] B. Harbecke, Appl. Phys. 39 (1986) 165-170

[18] B. Heinz, Optische Konstanten von Halbleiter-Mehrschichtsystemen (Diss. RWTH Aachen 1991)

[19] O. Stenzel, V. Hopke and P. Klobes, J. Appl. Phys. 24 (1991) 2088-2094

[20] A. R. Forouhi and I. Bloomer, Phys. Review 34 (1986) 7018-7026

[21] A. Eray and H. Tolunay, Material Science and Engineering 11 (1992) 47-50

[22] F. Zhu and J. Singh, Solar Enargy Materials and Solar Cells 31 (1993) 119-131

[23] F. Leblanc, J. Perrin and E. Cornil, J. Non-Cryst. Solids 137&138 (1991) 1165-1168

[24] F. B. Ellis Jr and A. E. Delahoy, (North-Holland Physics Publishing, 1985 printed from Solar Energy materials)

[25] G. D: Cody, B. G. Brooks and B. Abeles, Solar Energy Materials 8 (1982) 231-240

[26] C.Riordan and R. Hulstrom, Proc. of 21st IEEE OVSC (1990) 1085-1088